

Lawrence Berkeley National Laboratory

LBL Publications

Title

Energy-Degeneracy-Driven Covalency in Actinide Bonding

Permalink

<https://escholarship.org/uc/item/74g4q2g1>

Journal

Journal of the American Chemical Society, 140(51)

ISSN

0002-7863

Authors

Su, Jing

Batista, Enrique R

Boland, Kevin S

et al.

Publication Date

2018-12-26

DOI

10.1021/jacs.8b09436

Peer reviewed

ENERGY-DEGENERACY DRIVEN COVALENCY IN ACTINIDE BONDING

Jing Su,¹ Enrique R. Batista,^{1*} Sharon E. Bone,¹ Kevin S. Boland,¹ Joseph A. Bradley,^{1,2} Samantha K. Cary,¹ David L. Clark,^{1*} Steven D. Conradson,^{1,3} Alex S. Ditter,^{1,2} Jason M. Keith,^{1,4} Andrew Kerridge,⁵ Matthias W. Loeble,¹ Richard L. Martin,¹ Stefan G. Minasian,^{1,6} Veronika Mocko,¹ Henry S. La Pierre,¹ Nikolas Kaltsoyannis,⁷ Stosh A. Kozimor,^{1*} Marianne P. Wilkerson,¹ Laura E. Wolfsberg,¹ Gerald T. Seidler,² David K. Shuh,⁶ Ping Yang^{1*}

¹Los Alamos National Laboratory, P.O. Box 1663, Los Alamos, NM, 87545, United States

²University of Washington, Seattle, Washington 98195, United States

³Current Address: Washing State University and Matt, Institut Jozef Stefan.

⁴Current Address: Colgate University, Hamilton, New York 13346, United States

⁵Current Address: Lancaster University, Lancaster, LA1 4BE, United Kingdom

⁶Lawrence Berkeley National Laboratory, Berkeley, CA, 94720, United States

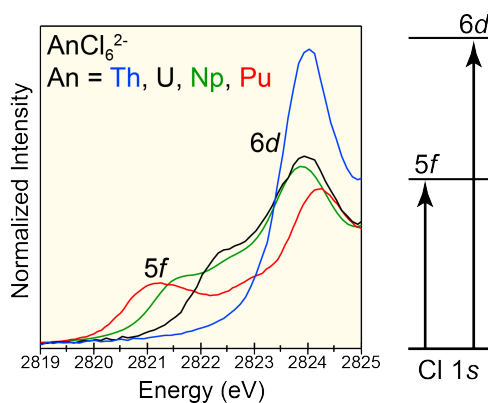
⁷School of Chemistry, The University of Manchester, Oxford Road, Manchester M13 9PL, United Kingdom

*To whom correspondence should be directed.

e-mail; erb@lanl.gov, dlclark@lanl.gov, stosh@lanl.gov, pyang@lanl.gov

TABLE OF CONTENT GRAPHIC

Covalent An–Cl bonding in series of +4 actinide hexachlorides, AnCl_6^{2-} ($\text{An}^{\text{IV}} = \text{U}, \text{Th}, \text{Np}, \text{Pu}$) have been characterized using Cl K-edge XAS and DFT. The results suggest that the 6d-orbital mixing is more substantial than that of the 5f-orbital. Additionally, the results indicate that 5f-covalent bonding with the Cl 3p orbitals is more substantial for Pu than for Th, U, and Np.



J. Su, E. R. Batista, S. E. Bone, K. S. Boland, J. A. Bradley, S. K. Cary, D. L. Clark, S. D. Conradson, A. S. Ditter, J. M. Keith, M. W. Loeble, N. Kaltsoyannis, S. A. Kozimor, M. P. Wilkerson, L. E. Wolfsberg, G. T. Seidler, D. K. Shuh, P. Yang.

Page No. – Page No.

Energy-Degeneracy Driven
Covalency in Actinide Bonding

KEYWORDS

actinium • plutonium • neptunium • uranium • thorium • Cl K-edge XAS • TDDFT • XANES

Abstract (Word Count: 119):

Evaluating the nature of chemical bonding for actinide elements represents one of the most important and longstanding problems in actinide science. We directly address this challenge and contribute a Cl K-edge X-ray absorption spectroscopy (XAS) and relativistic density functional theory (DFT) study that quantitatively evaluates An–Cl covalency in AnCl_6^{2-} ($\text{An}^{\text{IV}} = \text{Th}, \text{U}, \text{Np}, \text{Pu}$). The results showed significant mixing between Cl $3p$ - and An^{IV} $5f$ - and $6d$ -orbitals (t_{1u}^*/t_{2u}^* and t_{2g}^*/e_g^*), with the $6d$ -orbitals showing more pronounced covalent bonding than the $5f$ -orbitals. Moving from Th to U, Np, and Pu markedly changed the amount of M–Cl orbital mixing, causing An^{IV} $6d$ - and Cl $3p$ -mixing to decrease. Meanwhile, metal $5f$ - and Cl $3p$ -orbital mixing increased across this series.

Covalency(1) is a fundamental concept for rationalizing many chemical and physical phenomena. In contrast to transition d -elements where metal-ligand orbital mixing and overlap is well established, covalent bonding for plutonium (Pu) and the other actinides (An) has been debated for decades. For example, there is a body of evidence that demonstrates – in certain systems – substantial $5f$ - and $6d$ -covalency exists.(2–20) These data are juxtaposed with numerous studies suggesting that An–ligand bonding is primarily ionic.(21) The later conclusions are fueled by several observables that include (but are not limited to) An–ligand bond distances being routinely predicted using actinide ionic radii and an appreciable body of spectroscopic data that shows the

$5f \rightarrow 5f$ optical transitions are marginally impacted by the ligand field. Reconciling these observables and quantifying $5f$ - versus $6d$ -participation in covalent bonding represents one of the most longstanding and important fundamental problems in actinide science.

To directly address these challenges in actinide bonding, we have characterized covalency for Pu^{IV} and the other early actinides (Th^{IV} , U^{IV} , Np^{IV}) within an $O_h\text{-AnCl}_6^{2-}$ framework using a combination of ligand K-edge X-ray absorption spectroscopy (XAS)(22) and spin-orbit density functional theory (DFT) transition dipole-moment calculations.(9, 23–25) This duo has recently emerged as one of the most powerful approaches for characterizing metal–ligand covalency. For example, ligand K-edge XAS probes dipole-allowed bound-state transitions from the ligand $1s$ -orbitals to molecular orbitals that contain ligand p -character resulting from metal–ligand orbital mixing. As a result, the transition intensity in the ligand K-edge XAS measurement is directly related to the metal–ligand orbital mixing coefficient. For several reasons, we used this spectroscopic and computational approach to evaluate electronic structure and bonding in the highly symmetric AnCl_6^{2-} dianions. First, for many elements, octahedral metal complexes provide the foundation upon which understanding for a vast majority of metal–ligand bonding interactions exist. Second, the ubiquity of the $O_h\text{-MCl}_6^{x-}$ structure enables M–Cl covalency to be quantitatively evaluated across the periodic table as a function of the metal identity, *e.g.* among actinides, lanthanides, main group, and d -block transition elements. Third, within the AnCl_6^{2-} platform $5f$ - and $6d$ -hybridization is forbidden, owing to the selection rules governing octahedral symmetry. Hence, $5f$ - versus $6d$ -orbital orbital mixing can be discretely probed. We observed the An^{IV} $6d$ -orbitals participate in covalent bonding to a larger extent than the $5f$ -orbitals and that $5f$ -orbital mixing increased across the actinide series (from Th to Pu). The results are presented in the context

of an energy-degeneracy driven covalency concept, which provides understanding of roles that $5f$ - and $6d$ -orbital play in chemical bonding.

The $(\text{PPh}_4)_2\text{AnCl}_6^{2-}$ ($\text{An} = \text{Th}, \text{U}, \text{Pu}$) and $(\text{NMe}_4)_2\text{AnCl}_6$ ($\text{An} = \text{Th}, \text{U}, \text{Np}, \text{Pu}$) salts, hereafter referred to as AnCl_6^{2-} , were characterized by Cl K-edge XAS. The identity of the NMe_4^{1+} and PPh_4^{1+} had no substantial impact on the Cl K-edge XAS spectra. Complexes were prepared by previously reported synthetic procedures and isolated as large single crystals.(26, 27) The hexahalide salts contained large organic cations that guarded against $\text{An}-\text{Cl}\cdots\text{An}$ bridging interactions common in inorganic salts. This ensured that the $\text{An}-\text{Cl}$ bond was probed independently in the Cl K-edge XAS measurement. Background subtracted and normalized Cl K-edge XAS from AnCl_6^{2-} were compared in Figure 1. The four spectra were similar in that they contained a sharp edge-peak at high energy (~ 2828 eV) superimposed on an absorption threshold. The energies, intensities, and line shapes for these edge peaks were similar. For instance, the edge peak energies ranged from 2827.4 to 2827.6 eV, the peak maxima spanned 1.50 to 1.52, and the rising edge slopes varied from 0.4 to 0.6 eV^{-1} . For UCl_6^{2-} , these data were consistent with previous reports,(20) which highlighted the reproducibility of these measurements.

Although the edge region of the Cl K-edge XAS spectra was primarily invariant upon moving from Th to U, Np, and Pu, substantial changes were observed at low energy in the pre-edge spectral region, < 2826 eV. For instance, the spectrum from ThCl_6^{2-} contained a single pre-edge feature near 2824 eV (labeled **A**). Data from U, Np, and Pu also contained this **A** peak, albeit its intensity systematically decreased across the series. Moving from Th to Pu also caused additional pre-edge peaks to emerge at lower energy. For UCl_6^{2-} a second peak (labeled **B**) was present near 2822 eV and for NpCl_6^{2-} and PuCl_6^{2-} a third peak (labeled **C**) was apparent at ~ 2821 eV. In this sense, these AnCl_6^{2-} spectra were reminiscent to those from d -block metal tetrachlorides, MCl_4^{x-} ($\text{M} = \text{Co}^{\text{II}}$,

Ni^{II}, Co^{II}, Fe^{II}, Fe^{III}), studied previously by *SOLOMON* and *COWORKERS*. In both systems the number of pre-edge peaks in the Cl K-edge XAS spectra increased with increasing valence-electron count.(28) For Th^{IV} ($5f^0$), U^{IV} ($5f^2$), Np^{IV} ($5f^3$), and Pu^{IV} ($5f^4$), the increased number of pre-edge features was likely associated with appreciable multiplet and spin-orbit coupling contributions, all of which increase from Th to Pu.

Of particular significance were the spectra from Np and Pu, as these data represented the first time pre-edge features had been observed by ligand K-edge XAS spectroscopy, for these elements. We remind the reader that the pre-edge transition intensities are directly related to the M–Cl mixing coefficient.(22) Hence, the existence of these pre-edge peaks in Cl K-edge XAS from NpCl₆²⁻ and PuCl₆²⁻ provided unambiguous evidence for covalency in the Np–Cl and Pu–Cl bonds. The series of spectra also highlighted substantial diversity in electronic structure from Th to Pu. To quantify differences in An–Cl orbital mixing in AnCl₆²⁻, the pre-edge peaks and the edge features were deconvoluted with symmetrically constrained functions consisting of fixed 1:1 Lorentzian to Gaussian contributions. Our analyses also modeled the absorption threshold with a 1:1 mixture of arctangent to error function contributions. The curve fits agreed well with the experimental data, as shown by the low correlation coefficient, residual data that deviated from zero by less than 5% in the spectral region of interest, and symmetric residual peaks that were similar in shape to their parent Gaussian functions. The curve fitting models (Table 1 and Figure 2) showed that the peak intensities were consistent with the qualitative discussion above. For instance, the high-energy pre-edge **A** peaks near 2824 eV became less intense upon moving from Th to U, Np, and Pu, 1.26(6), 1.09(5), 1.05(5), 0.84(4). Similarly, the intermediate energy pre-edge **B** peaks near 2822 eV decreased in intensity from 0.40(2) (U) to 0.24(1) (Np) and 0.21(1) (Pu). Finally, the **C** peaks increased in intensity from 0.22(1) for Np to 0.36(2) for Pu. These curve fitting results indicated

that when moving from Th to Pu covalency did not uniformly change for every An–Cl interaction. The data instead showed that changes in actinide identity increased covalency in some An–Cl bonds and decreased covalency in other bonds.

To better understand the implications of the Cl K-edge XAS results described above, ground state scalar relativistic (SR) and spin-orbit (SO) density functional theory (DFT) calculations were used to guide the interpretation of the AnCl_6^{2-} spectra. The calculations were interpreted in accordance with well-established group theory descriptions of octahedral complexes. An example was provided in Figure 3 for ThCl_6^{2-} with relevant molecular orbitals visualized in Figure S1. The energy of the Th and Cl atomic orbitals were shown on the left side of this graphic. Allowing the orbitals to mix generated six symmetry-adapted linear combinations (SALCs) of Cl $3p$ -atomic orbitals of σ -symmetry ($a_{1g} + t_{1u} + e_g$) and twelve of π -symmetry ($t_{2g} + t_{1g} + t_{1u} + t_{2u}$) with respect to the Th–Cl bonds. As discussed previously, the metal $6d$ -atomic orbitals split as e_g and t_{2g} and were allowed by symmetry to form high energy M–Cl σ - and π -bonds, respectively (Figure 3). Meanwhile, at lower energy, the six actinide $5f$ -atomic orbitals of t_{1u} and t_{2u} symmetries mixed to form An–Cl $\sigma + \pi$ and π -bonds, respectively. This left the actinide a_{2u} orbital as rigorously non-bonding and the Cl t_{1g} orbitals as a set of non-bonding chlorine lone pairs.

Incorporating spin-orbit coupling into the calculations decreased orbital energy degeneracy, increased the energy range spanned by the $5f$ - and $6d$ -orbitals, and hybridized the valence orbitals. For example, in the scalar calculation for Th–Cl there was a non-bonding orbital of a_{2u} symmetry. Incorporating spin-orbit coupling appreciably hybridized this non-bonding orbital with the t_{2u} orbital. Spin-orbit coupling also blended the t_{1u} and t_{2u} orbitals, such that a purely t_{2u} state was nonexistent. Note, there was a high energy $5f$ -orbital of $e_{\frac{1}{2}u}$ symmetry whose composition was solely t_{1u} . As depicted in the calculated energy-level diagram shown in Figure 4, moving from Th

($5f^0$) to U ($5f^2$), Np ($5f^3$), and Pu ($5f^4$) did not significantly impact the energy of the $6d$ -orbitals. These $6d$ -orbitals were split into two groups, one near ~ 7 eV and a higher energy group near 10 eV. Meanwhile, moving across the series had marked influence on the $5f$ -orbitals, most notably by broadening the $5f$ -orbital regime from approximately 1 eV for ThCl_6^{2-} to approximately 6.5 eV for PuCl_6^{2-} .

These ground state calculations were used to compute the Cl core electron excitation spectrum using a first order approximation on the basis of the transition dipole between initial and final state and the excitation energies obtained from the occupied and unoccupied orbital energies. The agreement between prediction (Figure 5) and the experimental spectra engendered an electronic structure based interpretation of the AnCl_6^{2-} Cl K-edge XAS spectra. For instance, simulated AnCl_6^{2-} spectra (Figure 5) reproduced the pre-edge features in the experimental spectra and were consistent with group theoretical analyses. The calculations suggested that the pre-edge peaks stemmed from electronic excitations from Cl $1s$ -orbitals to unoccupied orbitals that resulted from mixing between Cl $3p$ -orbitals and the An^{IV} $5f$ - and $6d$ -orbitals. For ThCl_6^{2-} , the transitions to $5f$ - and $6d$ -orbitals were very close in energy. Experimentally, only a single **A** peak was observed whose origin was attributed to transitions to antibonding orbitals that resulted from covalent mixing between the Cl $3p$ - and Th $5f$ - and $6d$ -orbitals. The calculations also indicated that transitions to higher lying $6d$ -orbitals (e_g^* in the scalar calculations) were higher in energy and beyond the rising edge. For UCl_6^{2-} , NpCl_6^{2-} , and PuCl_6^{2-} , the calculations revealed that the high energy **A** peaks (2824 eV) were almost exclusively associated with Cl $1s$ -electronic excitations to $6d$ -orbitals. Computational results additionally suggested that transitions to $5f$ -orbitals could be resolved from the $6d$ -orbitals for UCl_6^{2-} , NpCl_6^{2-} , and PuCl_6^{2-} . For example, in the UCl_6^{2-} case, the computational results attributed the **B** peak to electronic excitations from Cl $1s$ -orbitals to the

antibonding $5f$ -orbitals (those of t_{1u}^* and t_{2u}^* parentage in the scalar calculations). Moving to NpCl_6^{2-} broadened the energy range for these $\text{Cl } 1s \rightarrow \text{An}^{\text{IV}} 5f$ -transitions and split the feature into two peaks, consistent with the experimental observations. Finally, moving from NpCl_6^{2-} to PuCl_6^{2-} further broadened the energy range over which transitions to $5f$ -orbitals spanned. Again, this prediction was consistent with experiment. Note, while compiling this computational and experimental work, *DE JONG* and *COWORKERS* published their own independent calculations after we communicated structural and spectroscopic information.(29) Their results were consistent with the experimental and theoretical results we presented at multiple meetings.(30–35)

Comparing the AnCl_6^{2-} Cl K-edge XAS pre-edge intensities showed similar trends in orbital mixing as obtained from the calculations (Figure S2). These two comparisons suggested that covalency in bonding between the Cl $3p$ - and $\text{An}^{\text{IV}} 6d$ -orbitals was larger than with the $\text{An}^{\text{IV}} 5f$ -orbitals. Perturbation theory provided a platform for rationalizing this observation. Recall that the orbital mixing coefficient (λ) is directly related to coupling matrix element between metal and ligand (H_{ML}) and inversely related to the energy difference between the metal and ligand valence orbitals ($E_M^0 - E_L^0$).

$$\lambda = \frac{H_{ML}}{E_M^0 - E_L^0} \quad (1)$$

Consistent with the distribution of radial densities of actinide $5f$ -, $6d$ -, and Cl $3p$ -orbitals (Figure S3) and the corresponding orbital overlap (Figure S4), our results suggested that the more extended $\text{An}^{\text{IV}} 6d$ -orbitals were more available to mix with the Cl $3p$ -valence than the contracted $\text{An}^{\text{IV}} 5f$ -orbitals. Hence, the coupling term (H_{ML}) seemed most important in directing $\text{An}^{\text{IV}} 6d$ - vs. $5f$ -orbital mixing with Cl $3p$ -orbitals. These observations were consistent with numerous accounts suggesting that limited $5f$ -orbital radial distributions cause small H_{ML} , which in turn can limit $5f$ -orbital participation in covalent bonding.(5, 16, 36)

The H_{ML} term decreases from Th to Pu, owing to the $5f$ -orbital radial density decreasing from Th^{IV} to Pu^{IV} (Figure S4). This decrease in orbital overlap should accompany decreased An–Cl orbital mixing. However, the experimental and computational results showed that An^{IV} $5f$ and Cl $3p$ -orbital mixing increased – not decreased – when moving from Th^{IV} to Pu^{IV} . We rationalize the observed increase by considering the denominator of Eq. 1 ($E_{\text{M}}^0 - E_{\text{L}}^0$).^(20, 37) For example, moving from Th to Pu decreases the energy of the $5f$ -orbitals (Figure 4), making them better matched (energetically) with the Cl $3p$ -orbitals. In this case, the more favorable energy degeneracy orbital term ($E_{\text{M}}^0 - E_{\text{L}}^0$) outweighs the negative impact from H_{ML} , thereby providing a mechanism to increase An^{IV} $5f$ -covalency for Pu relative to Th. This route to covalent $5f$ -bonding is an alternative to the more conventional H_{ML} pathways commonly invoked to rationalize orbital mixing in transition metal and main group elements.^(20, 38–42)

Determining the relative participation of $5f$ - and $6d$ -orbitals in actinide bonds is a long-standing experimental and computational challenge in fundamental actinide physics and chemistry.⁽³⁷⁾ Herein, we addressed this challenge and characterized actinide $5f$ - versus $6d$ -mixing with Cl $3p$ -orbitals in the An^{IV}Cl₆²⁻ salts. The experimental and computational results showed transitions in the Cl K-edge XAS from UCl₆²⁻, NpCl₆²⁻, and PuCl₆²⁻ that were a direct result of actinide $5f$ - and $6d$ - mixing with Cl $3p$ -orbitals. The results revealed that the $6d$ -orbitals participated in covalent bonding to a larger extent than the $5f$ -orbitals (Table 1). Additionally, $5f$ - and $6d$ - participation in covalent bonding followed opposite trends across the early tetravalent actinide series ($5f$ increased and $6d$ decreased). Combined, the experimental and theoretical results agreed that $5f$ -participation in covalent bonding was largest for Pu, intermediate for Np and U, and lowest for Th. This observation resulted from Cl $3p$ -orbital energies matching the $5f$ -orbitals of Pu better than those of Np, U, and Th. These results support the idea that f -orbital mixing is heavily

influenced by energy-degeneracy driven covalency. This aspect of the An–Cl bonding highlights a uniqueness associated with actinide electronic structure bonding, not typically considered as a dominate parameter for other elements on the periodic table. Excited by these observations, we are currently exploring the possibility of using concepts of energy-degeneracy driven covalency to access more pronounced $5f$ -orbital mixing in other systems.

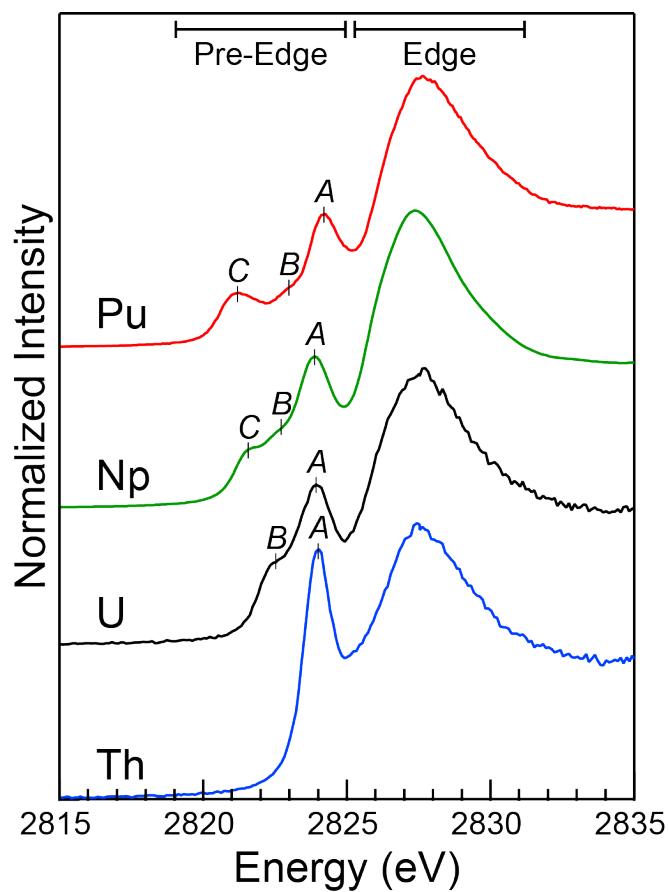


Figure 1: The normalized and background subtracted Cl K edge XAS spectra from AnCl_6^{2-} ($\text{An}^{\text{IV}} = \text{Th}, \text{U}, \text{Np}, \text{Pu}$).

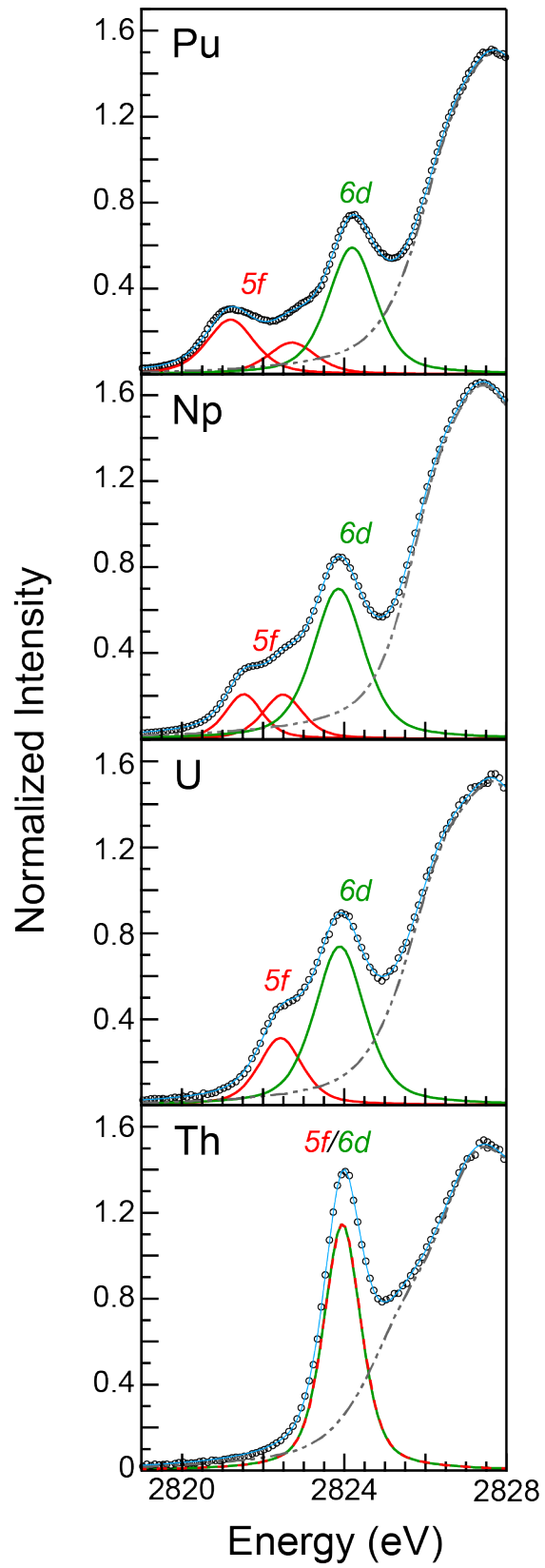


Figure 2: The Cl–K edge XAS data and deconvoluted spectra for AnCl_6^{2-} ($\text{An}^{\text{IV}} = \text{Th}, \text{U}, \text{Np}, \text{Pu}$) are shown. Experimental data is shown in circles (\circ), a 0.5:0.5 ratio of Lorentzian and Gaussian functions is used to model the pre–edge features are shown as red and green traces. The summed curve fit is shown as light blue trace, the residual edge function is shown as interrupted brown trace.

Table 1. A comparison of experimental and calculated pre-edge peak energies (eV), intensities, and % Cl 3*p* character^a for AnCl₆²⁻ (An^{IV} = Th, U, Np and Pu) dianions.^a

Compound	A Peak			B peak			C peak		
	Energy	Int.	% Cl 3 <i>p</i>	Energy	Int	% Cl 3 <i>p</i>	Energy	Int	% Cl 3 <i>p</i>
<i>D</i> _{2<i>d</i>} -Cs ₂ CuCl ₄ ³⁵	2820.20	0.53	7.53	–	–	–	–	–	–
ThCl ₆ ¹⁻	2824.0	1.26	17.9	–	–	–	–	–	–
UCl ₆ ¹⁻	2823.9	1.09	15.5	2822.4	0.40	5.6	–	–	–
NpCl ₆ ¹⁻	2823.9	1.05	14.9	2822.5	0.24	3.4	2821.53	0.22	3.1
PuCl ₆ ¹⁻	2824.2	0.84	11.9	2822.7	0.21	3.0	2821.2	0.36	5.1

^aThe percent Cl 3*p* character was reported per M–Cl bond (M=Cu, Th, U, Np and Pu).

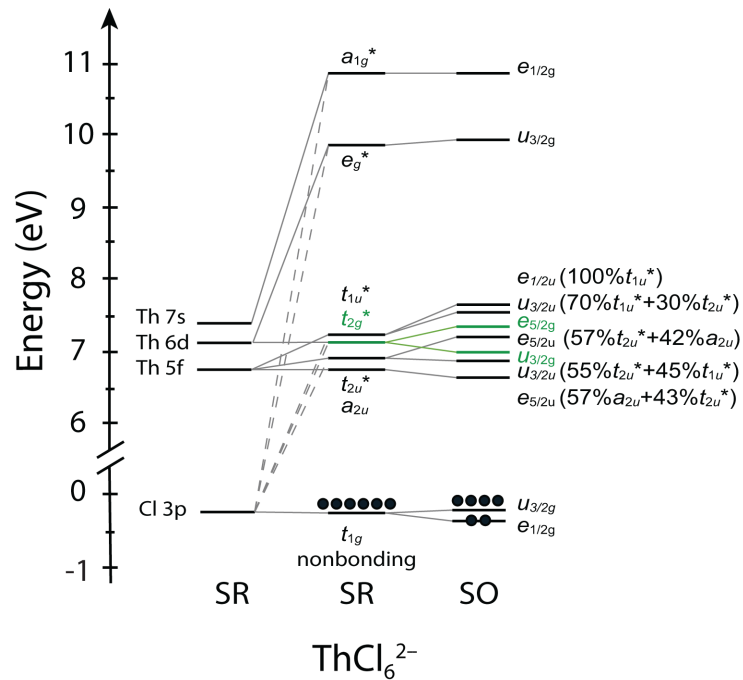


Figure 3. Energy level diagram from DFT ground-state calculations for the ThCl_6^{2-} . *Left* – atomic orbitals from scalar relativistic (SR) calculations. *Center* – orbitals for ThCl_6^{2-} from SR calculations. *Right* – orbitals for ThCl_6^{2-} from calculations that incorporate spin-orbit (SO) coupling.

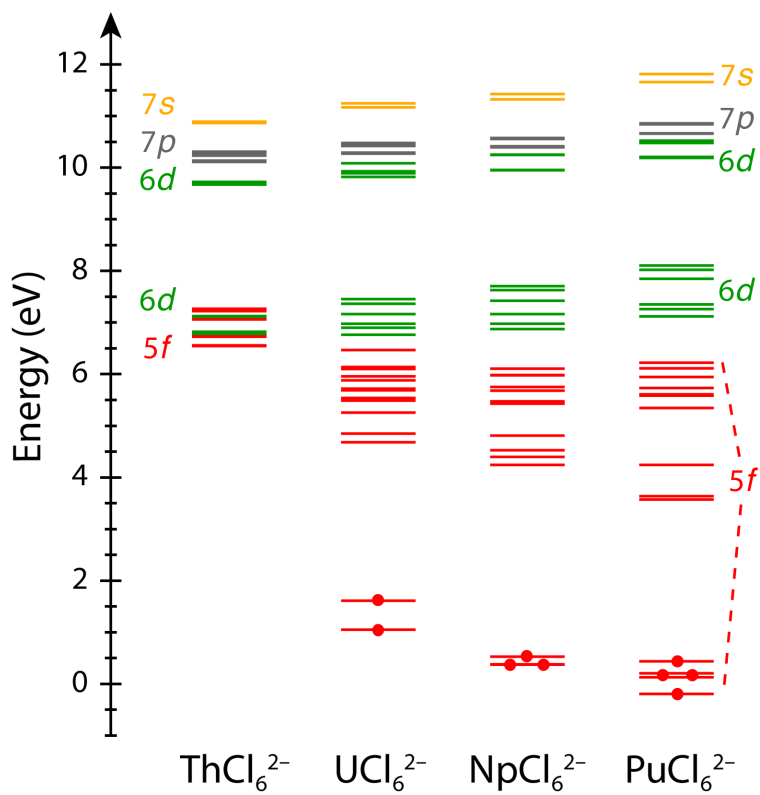


Figure 4. Energy level diagram from DFT ground-state calculations that incorporate spin-orbit coupling showing the progression from ThCl_6^{2-} to PuCl_6^{2-} .

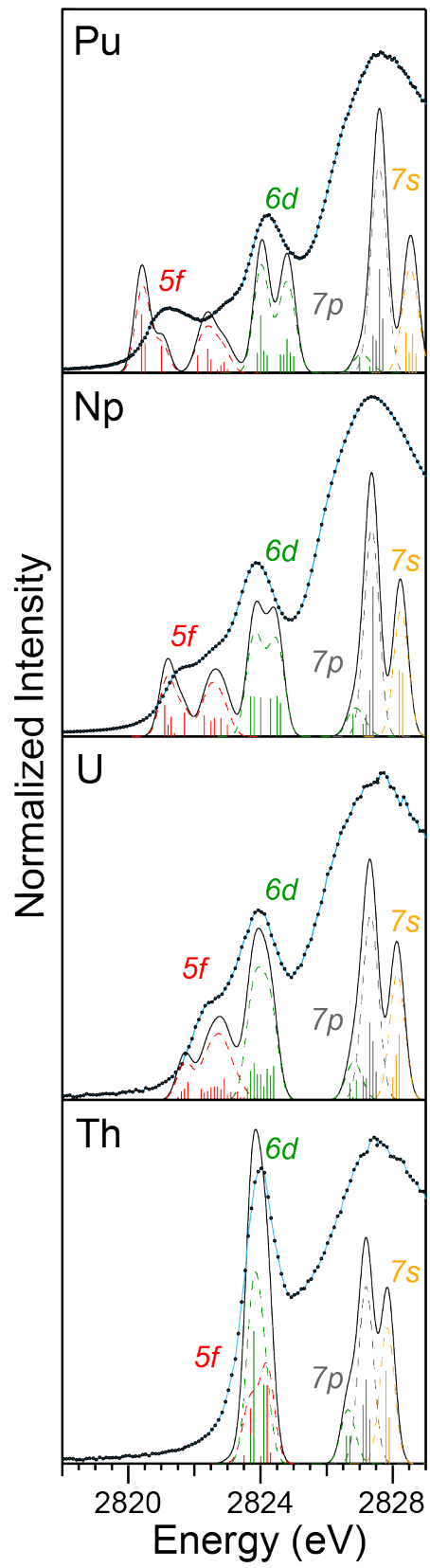


Figure 5. Comparison between experimental Cl K-edge XAS Spectra (●) and results from the spin-orbit DFT transition dipole moment calculations (black trace) for the AnCl_6^{2-} ($\text{An}^{\text{IV}} = \text{Th}, \text{U}, \text{Np}, \text{Pu}$) dianions. The red, green, yellow and gray bars and dashed traces represent the energy and oscillator strength for the calculated transitions involving 5f-, 6d-, 7s- and 7p-final states, respectively.

References

1. W. Heitler, F. London, Wechselwirkung neutraler Atome und homöopolare Bindung nach der Quantenmechanik. *Physics (College. Park. Md)*. **44**, 455–472 (1927).
2. R. M. Diamond, K. Street, G. T. Seaborg, An Ion-exchange Study of Possible Hybridized 5f Bonding in the Actinides. *J. Am. Chem. Soc.* **76**, 1461–1469 (1954).
3. Karraker D. G., J. A. Stone, E. R. Jones, N. Edelstein, Bis (cyclooctatetraenyl) neptunium(IV) and Bis (cyclooctatetraenyl) plutonium(IV). *J. Am. Chem. Soc.* **92**, 4841–4845 (1970).
4. W. W. Lukens *et al.*, Quantifying the σ and π interactions between U(V) f orbitals and halide, alkyl, alkoxide, amide and ketimide ligands. *J. Am. Chem. Soc.* **135**, 10742–10754 (2013).
5. N. Kaltsoyannis, Does covalency increase or decrease across the actinide series? Implications for minor actinide partitioning. *Inorg. Chem.* **52**, 3407–3413 (2013).
6. S. G. Minasian *et al.*, New evidence for 5f covalency in actinocenes determined from carbon K-edge XAS and electronic structure theory. *Chem. Sci.* **5** (2014), doi:10.1039/c3sc52030g.
7. M. W. Löble *et al.*, Covalency in Lanthanides. An X-ray Absorption Spectroscopy and Density Functional Theory Study of LnCl₆ x - (x = 3, 2). *J. Am. Chem. Soc.* **137**, 2506–2523 (2015).
8. A. Formanuk *et al.*, Actinide covalency measured by pulsed electron paramagnetic resonance spectroscopy. *Nat. Chem.* **9**, 578–583 (2016).
9. J. N. Cross *et al.*, Covalency in Americium(III) Hexachloride. **139**, 8667–8677 (2017).
10. M. P. Kelley *et al.*, Bond Covalency and Oxidation State of Actinide Ions Complexed with Therapeutic Chelating Agent 3,4,3-LI(1,2-HOPO). *Inorg. Chem.* **57**, 5352–5363 (2018).
11. D.-C. Sergentu, F. Gendron, J. Autschbach, *Chem. Sci.*, in press, doi:10.1039/C7SC05373H.
12. N. Kaltsoyannis, Transuranic Computational Chemistry. *Chem. - A Eur. J.* **24**, 2815–2825 (2018).
13. A. Avdeef, K. N. Raymond, K. O. Hodgson, A. Zalkin, Two Isostructural Actinide π Complexes. The Crystal and Molecular Structure of Bis(cyclooctatetraenyl)uranium(IV), U(C₈H₈)₂, and Bis(cyclooctatetraenyl)thorium(IV), Th(C₈H₈)₂. *Inorg. Chem.* **11**, 1083–1088 (1972).
14. J. P. Clark, J. C. Green, The He-1 Photoelectron Spectra of Uranocene and Thorocene. *J. Organomet. Chem.* **112**, C14–C16 (1976).
15. K. Tatsumi, A. Nakamura, P. Hofmann, P. Stauffert, R. Hoffmann, Carbon monoxide activation by biscyclopentadienyl complexes of Group 4 metals and actinides: .eta.2-acyl complexes. *J. Am. Chem. Soc.* **107**, 4440–4451 (1985).
16. M. Pepper, B. E. Bursten, The Electronic Structure of Actinide-Containing Molecules: A Challenge to Applied Quantum Chemistry. *Chem. Rev.* **91**, 719–741 (1991).
17. M. Straka, M. Patzschke, P. Pyykkö, Why are hexavalent uranium cyanides rare while U-F and U-O bonds are common and short? *Theor. Chem. Acc.* **109**, 332–340 (2003).
18. R. G. Denning, Electronic Structure and Bonding in Actinyl Ions. *J. Phys. Chem. A.* **111**, 4125–4143 (2007).

19. I. D. Prodan, G. E. Scuseria, R. L. Martin, Covalency in the actinide dioxides: Systematic study of the electronic properties using screened hybrid density functional theory. *Phys. Rev. B*. **76**, 33101 (2007).
20. S. G. Minasian *et al.*, Determining relative f and d orbital contributions to M-Cl covalency in MCl₆²⁻ (M = Ti, Zr, Hf, U) and UOCl₅-using Cl K-edge X-ray absorption spectroscopy and time-dependent density functional theory. *J. Am. Chem. Soc.* **134** (2012), doi:10.1021/ja2105015.
21. J. V Beitz, G. Liu, in *The Chemistry of the Actinide and Transactinide Elements*, L. Morss, N. Edelstein, J. Fuger, Eds. (Springer: Berlin, 2006), p. 2013.
22. E. I. Solomon, B. Hedman, K. O. Hodgson, A. Dey, R. K. Szilagy, Ligand K-edge X-ray absorption spectroscopy: Covalency of ligand-metal bonds. *Coord. Chem. Rev.* **249**, 97–129 (2005).
23. M. Casarin, P. Finetti, A. Vittadini, F. Wang, T. Ziegler, Spin - orbit relativistic time-dependent density functional calculations of the metal and ligand pre-edge XAS intensities of organotitanium complexes: TiCl₄, Ti(η^5 -C₅H₅)Cl₃, and Ti(η^5 -C₅H₅)₂Cl₂. *J. Phys. Chem. A*. **111**, 5270–5279 (2007).
24. S. A. Kozimor *et al.*, Trends in Covalency for d- and f-Element Metalloocene Dichlorides Identified Using Chlorine K-Edge X-ray Absorption Spectroscopy and Time-Dependent Density Function Theory. *J. Amer. Chem. Soc.* **131**, 12125–12136 (2009).
25. F. Neese, Software update: the ORCA program system, version 4.0. *Wiley Interdiscip. Rev. Comput. Mol. Sci.* **8**, 4–9 (2018).
26. S. G. Minasian *et al.*, Synthesis and structure of (Ph₄P)₂MCl₆ (M = Ti, Zr, Hf, Th, U, Np, Pu). *Inorg. Chem.* **51**, 5728–36 (2012).
27. A. M. Mounce *et al.*, Nuclear Magnetic Resonance Measurements and Electronic Structure of Pu(IV) in [(Me)₄N]₂PuCl₆. *Inorg. Chem.* **55**, 8371–8380 (2016).
28. S. E. Shadle, B. Hedman, K. O. Hodgson, E. I. Solomon, Ligand K-Edge X-ray Absorption Spectroscopic Studies: Metal-Ligand Covalency in a Series of Transition Metal Tetrachlorides. *J. Am. Chem. Soc.* **117**, 2259–2272 (1995).
29. N. Govind, W. A. de Jong, Simulating Cl K-edge X-ray absorption spectroscopy in MCl₆²⁻ (M = U, Np, Pu) complexes and UOCl₅- using time-dependent density functional theory. *Theor. Chem. Acc.* **133**, 1–7 (2014).
30. P. Yang *et al.*, (2007), p. NUCL-120.
31. D. L. Clark *et al.*, (2008), p. NUCL-048.
32. E. R. Batista *et al.*, in *ACS National meeting, Washington, DC* (2009), p. NUCL-178.
33. D. L. Clark *et al.*, (2009), p. NUCL-119.
34. D. L. Clark *et al.*, (2011), p. NUCL-16.
35. H. S. La Pierre *et al.*, (2015), p. INOR-643.
36. H. M. Crosswhite, H. Crosswhite, W. T. Carnall, A. P. Paszek, Spectrum analysis of U³⁺:LaCl₃. *J. Chem. Phys.* **72**, 5103–5117 (1980).
37. M. L. Neidig, D. L. Clark, R. L. Martin, Covalency in f-element complexes. *Coord. Chem. Rev.* **257**, 394–406 (2013).
38. S. G. Minasian *et al.*, Covalency in metal-oxygen multiple bonds evaluated using oxygen K-edge spectroscopy and electronic structure theory. *J. Am. Chem. Soc.* **135** (2013), doi:10.1021/ja310223b.
39. A. C. Olson *et al.*, Using solution- and solid-state S K-edge X-ray absorption spectroscopy with density functional theory to evaluate M-S bonding for MS₄²⁻ (M = Cr,

- Mo, W) dianions. *Dalt. Trans.* **43** (2014), doi:10.1039/c4dt02302a.
40. M. W. Löble *et al.*, Covalency in lanthanides. An X-ray absorption spectroscopy and density functional theory study of $\text{LnCl}_6^{\text{x-}}$ ($x = 3, 2$). *J. Am. Chem. Soc.* **137** (2015), doi:10.1021/ja510067v.
 41. M. J. Tassell, N. Kaltsoyannis, Organo-f-element catalysts for efficient and highly selective hydroalkoxylation and hydrothiolation. *Dalt. Trans.* **39**, 6576–6588 (2010).
 42. I. Kirker, N. Kaltsoyannis, Does covalency really increase across the 5f series? A comparison of molecular orbital, natural population, spin and electron density analyses of AnCp_3 ($\text{An} = \text{Th-Cm}$; $\text{Cp} = \eta^5\text{-C}_5\text{H}_5$). *Dalt. Trans.* **40**, 124–131 (2011).